CrossMark

Influence of annealing temperature on formation and photoelectric properties of AZO nanosheet-coated FTO-based films

Li-jing Huang[1,3] · Bao-jia Li[2,3] · Hai-di Cao[1,3] · Wei Zu[1,3] · Nai-fei Ren[1,3] · Hua Ding[3,4]

Abstract In this work, we reported a direct fabrication of Al-doped zinc oxide (AZO) nanosheets on fluorine-doped tin oxide (FTO)-based substrates using thermal annealing method. Specifically, silver (Ag) and AZO layers were successively deposited on commercial FTO/glass by direct current magnetron sputtering, and then the as-deposited AZO/Ag/FTO films were thermally annealed in a tube furnace to prepare AZO nanosheets. The effects of annealing temperature on the AZO nanosheet morphology and the performance of AZO/Ag/FTO films were investigated by an X-ray diffractometer, a scanning electron microscope, an energy dispersive spectrometer, optical transmittance spectra, reflectance spectra and a digital four-point probe instrument. It was found that a suitable temperature resulted in the formation of AZO nanosheets, which could effectively decrease the reflectance and thus improve the transmittance of the films. Smaller densely-distributed AZO nanosheets were observed on the film annealed at 450 °C, enabling it to have the highest average transmittance of 81.0% and the lowest reflectance of 6.3% in the waveband of 400–800 nm.

The results also showed that the film annealed at 450 °C had the highest figure of merit of 2.59×10^{-2} Ω^{-1}, which was more than four times that of the as-deposited film (0.57×10^{-2} Ω^{-1}). This work demonstrates the availability of preparing AZO nanosheets by thermal annealing and provides a reference for improving overall photoelectric property of transparent conducting oxide films.

1 Introduction

Fluorine-doped tin oxide (FTO), which is an important n-type wide-band gap transparent conducting oxide (TCO) film, has been widely used as transparent electrodes in optoelectronic devices because of its low cost, good thermal and chemical stability [1]. However, the existing performance (especially optical and electrical properties) of FTO films cannot meet the needs of the rapid development of optoelectronic device areas. In order to fit the demands for high performance, bilayer or multilayer composition through introducing ultrathin metal and/or semiconductor layers to obtain metal/TCO bilayer or TCO/metal/TCO multilayer films has been proposed by researchers [2, 3]. It is well known that silver (Ag) is the most electrically conductive metal, which has a large variety of potential applications and thus has been extensively investigated [4]. Al-doped zinc oxide (AZO), as an emerging TCO material that always acts as the upper layer in bilayer or multilayer transparent conducting films, has attracted more and more attention due to its rich storage, non-toxicity and specific optical and electrical properties [5, 6].

Generally, the introduction of metal and semiconductor layers will be more effective to improve conductivity of a single-layer TCO film, but the transmittance of the film decreases with the increase in thickness of the metal or

✉ Li-jing Huang
lij_huang@126.com

✉ Bao-jia Li
li_bjia@126.com

1 School of Mechanical Engineering, Jiangsu University, Zhenjiang 212013, People's Republic of China

2 School of Materials Science and Engineering, Jiangsu University, Zhenjiang 212013, People's Republic of China

3 Jiangsu Provincial Key Laboratory of Center for Photon Manufacturing Science and Technology, Jiangsu University, Zhenjiang 212013, People's Republic of China

4 School of Automobile and Traffic Engineering, Jiangsu University, Zhenjiang 212013, People's Republic of China

semiconductor layers [7, 8]. For the purpose of improving film transmittance, many researches have been focused on fabricating anti-reflective coatings with special nanostructures on TCO-based films. The existence of the nanostructures can reduce the light reflection on the film surfaces, so as to improve transmittance of the films and boost light utilization [9–11]. It has been reported that AZO has a diversity of nanostructures, such as nanowires [12], nanorods [13, 14], nanoneedles [15] and nanosheets [16]. The common methods for fabricating AZO nanostructures include hydrothermal growth [14, 15], wet etching [17], sol–gel technique [18] and chemical vapor deposition [19], etc. But all these methods involve dangerous chemicals, complex procedures, low processing efficiencies and rigorous experimental conditions. Therefore, it is important to find a simple, less toxic and controllable method for preparing AZO nanostructures. It has been reported that heating can promote the formation of ZnO nanostructures [20, 21]. Inspired by this result, heating of AZO films in a tube furnace is expected to give rise to the possibility of generating AZO nanostructures. Moreover, it is worth mentioning that heating in a tube furnace (so-called thermal annealing) can also enhance crystallinity of the films through promoting grain recrystallization, which will be conducive to improvement of the optical and electrical properties of the films [22, 23]. However, by now, there is no relevant experiment about applying thermal annealing on fabrication of AZO nanostructures that has been reported.

In this article, we investigated fabrication of AZO nanosheets on FTO-based films through thermal annealing and the morphology of the AZO nanosheets was regulated by annealing temperature. Specifically, Ag and AZO layers were successively deposited on commercial FTO/glass by direct current (DC) magnetron sputtering, and then the AZO/Ag/FTO films were annealed in a tube furnace to obtain AZO nanosheets. The effects of annealing temperature on the AZO layer morphology and the performance of the AZO/Ag/FTO films were also examined. The fabrication of AZO nanosheets is based on a straightforward and one-step heat-treatment approach, which can avoid some harmful chemicals and eliminate the nanostructure transfer process for multilayer film fabrication, providing a novel idea for preparing AZO nanosheets directly on FTO-based films.

2 Experiment

Ag and AZO layers were successively deposited on small pieces (15 mm × 15 mm) of FTO/glass (750 nm/3 mm) substrates by DC magnetron sputtering using Ag (99.99% purity) metallic and AZO (ZnO:Al$_2$O$_3$ = 95 wt%:5 wt%) ceramic targets without external heating. Prior to

deposition, the FTO/glass substrates were cleaned ultrasonically with deionized water, acetone and anhydrous ethanol each for 10 min and then dried by blowing high-purity (99.99%) nitrogen. The deposition chamber was evacuated to a base pressure of about 1×10^{-3} Pa and then introduced high-purity (99.99%) argon with a working pressure of 35 Pa. The thicknesses of the Ag and AZO layers were 5 and 150 nm, respectively, which were controlled by deposition time and monitored in situ by a quartz-crystal-based thickness monitor. Subsequently, the as-deposited AZO/Ag/FTO films were thermally annealed in a tube furnace at different temperatures (i.e. 300, 350, 400, 450 and 500 °C) under high-purity (99.99%) nitrogen atmosphere for 20 min and cooled naturally to room temperature. During thermal annealing, nitrogen with a flow rate of 10 sccm was introduced into the furnace chamber.

A scanning electron microscope (SEM, Hitachi 4800) and an energy dispersive spectrometer (EDS) were used to observe the top-view images of the films and analyze the composition of the coatings, respectively. The crystal phases of the films were characterized by an X-ray diffractometer (XRD, Bruker D8 Advance) using Cu-$K\alpha$ radiation ($\lambda = 0.1541$ nm) at 2θ mode. The optical transmittance and reflectance spectra of the films were measured using a spectrophotometer (Shanghai Yuanxi UV-6100). The sheet resistances of the films were measured by a digital four-point probe instrument (Guangzhou Four Probes Tech RTS-9). All tests were performed at room temperature.

3 Results and discussion

3.1 Crystal structure

Figure 1 presents the XRD patterns of various AZO/Ag/FTO films. The as-deposited and the annealed AZO/Ag/
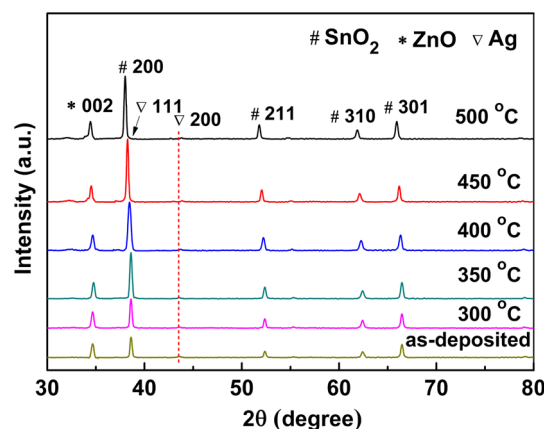
Fig. 1 XRD patterns of the as-deposited and the annealed AZO/Ag/FTO films under different temperatures

FTO films all contain the SnO_2 tetragonal structure (JCPDS no. 41-1445) and exhibit preferred orientation along the (200) plane. For the annealed AZO/Ag/FTO films, with increasing annealing temperature from 300 to 500 °C, the three main diffraction peaks of SnO_2 in the FTO layers, i.e. (200), (211) and (301), become stronger and narrower. Meanwhile, all the films also display the ZnO hexagonal structure (JCPDS no. 36-1451). It is notable that ZnO (002) peaks have the same changing trend as that of the SnO_2 (200), (211) and (301) peaks. These results indicate that increasing annealing temperature can promote the crystallization of the films and effectively reduce the defects in the films [24]. In addition, the as-deposited and the annealed AZO/Ag/FTO films all show the weak Ag (111) [overlapped with the SnO_2 (200) peak] and (200) peaks, confirming the presence of the Ag face-centered cubic phase (JCPDS no. 65-2871). The Debye–Scherrer formula [25], which was defined as follows, was adopted to calculate the average crystallite size (D) of the films.

$$D = \frac{0.9\lambda}{\beta \cos \theta_B}, \tag{1}$$

where λ is the X-ray wavelength (0.1541 nm), θ_B is the Bragg angle and β is the full width at half maximum (FWHM) of θ_B. The crystallite sizes of the AZO layers and the FTO layers for various films were determined from the main ZnO diffraction peak [i.e. (002)] and the three main SnO_2 diffraction peaks [i.e. (200), (211) and (301)], respectively. The calculated results are shown in Table 1. It is found that the crystallite sizes of the AZO layers and the FTO layers for all the annealed AZO/Ag/FTO films are significantly higher than those of the as-deposited film, implying that thermal annealing can effectively promote recrystallization of the films. Moreover, as the annealing temperature is elevated, the crystallite sizes of both the AZO layers and the FTO layers gradually increase, which is in agreement with the result presented by Kuo et al. [26].

3.2 Surface morphology

Figure 2 shows the top-view SEM images of the as-deposited and the annealed AZO/Ag/FTO films under different temperatures. In Fig. 2a, the surface of the as-

**Table 1** Crystallite sizes of the AZO and FTO layers obtained by XRD analysis for different AZO/Ag/FTO films

Sample	As-deposited	Annealing temperature (°C)				
		300	350	400	450	500
Crystallite size D (nm)						
AZO layer	18.5	21.9	23.1	23.7	26.6	26.9
FTO layer	26.2	31.3	32.7	32.8	34.1	34.8

deposited AZO/Ag/FTO film is found to be covered with small and uniform AZO particles that are densely distributed. After annealing at 300 °C, as Fig. 2b shows, the film surface begins to emerge a smaller number of AZO needlelike whiskers. In Fig. 2c, with increasing annealing temperature to 350 °C, the morphology of the whiskers becomes clearer and the number of the whiskers significantly increases. The whiskers begin to become thinner and gradually form curly AZO nanosheets after being annealed at 400 °C, as shown in Fig. 2d. The AZO needlelike whiskers translating into AZO nanosheets may be a result of the absorption of Al_2O_3 nanoparticles in the AZO layer on the ZnO (002) plane that can reduce the growth rate of ZnO crystals [27]. As Fig. 2e shows, densely-distributed AZO nanosheets are observed on the whole surface of the film annealed at 450 °C, and the sizes of the AZO nanosheets become smaller. It can also be seen in the inset that the AZO thin nanosheets are closely adhered onto the surface of the film. With the further increase in annealing temperature to 500 °C, as can be seen in Fig. 2f, the collapsed AZO nanosheets are compactly filled among the particles on the film surface, which can be explained by the evaporation of AZO under the higher temperature. In addition, by a detailed comparison, it can also be found that the AZO particles on all the annealed film surfaces are slightly larger than those on the as-deposited film surface. These evolutions are consistent with the XRD results and may be ascribed to the grain recrystallization caused by the thermal annealing effect [28]. To further confirm the chemical composition of the AZO/Ag/FTO film annealed at 450 °C, an EDS spectrum was recorded with an electron beam probe size of ~ 1 μm, as presented in Fig. 3. The spectrum clearly reveals that the film contained Sn, Zn, Al, O and Ag elements, suggesting the presence of SnO_2, ZnO, Al_2O_3 and Ag in the film.

3.3 Optical property

Figure 4 shows the transmittance spectra of the as-deposited and the annealed AZO/Ag/FTO films using different annealing temperatures. The optical absorption edges of all the annealed AZO/Ag/FTO films are strongly blue-shifted as compared to the as-deposited film, which reflects the increase of the carrier concentration blocking the lowest states in the conduction band [29]. The average transmittance (T_{av}) values were obtained by averaging the transmittance values in the visible waveband (400–800 nm) that extracted from the optical transmittance spectra, i.e. T_{av} was defined as [30]:

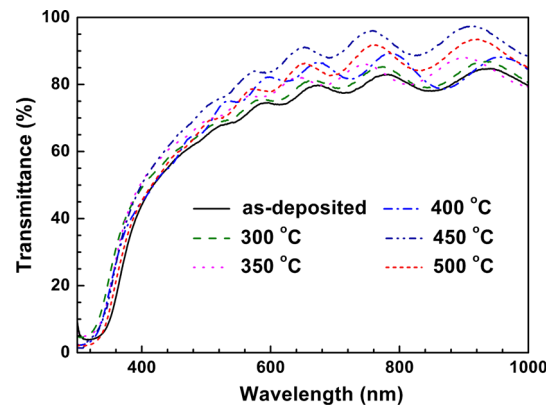$$T_{av} = \frac{\sum_{i=1}^{n} T_i}{n}, \tag{2}$$
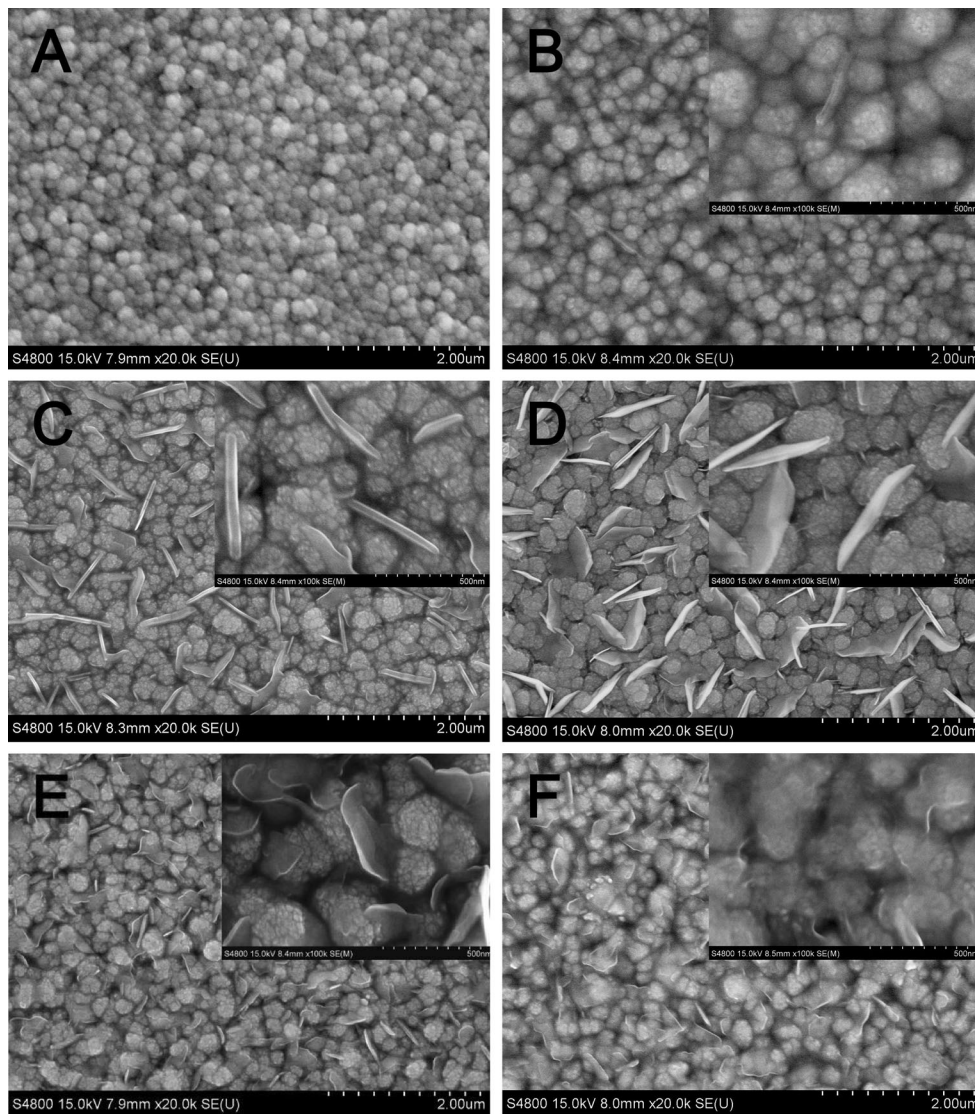
Fig. 2 Top-view SEM images of the as-deposited and the annealed AZO/Ag/FTO films under different temperatures: **a** as-deposited, **b** 300 °C, **c** 350 °C, **d** 400 °C, **e** 450 °C, **f** 500 °C (the *insets* show the high-magnification image of the corresponding films)
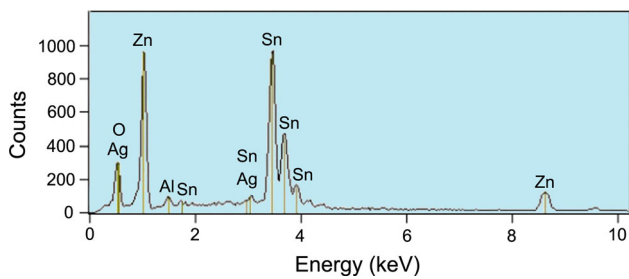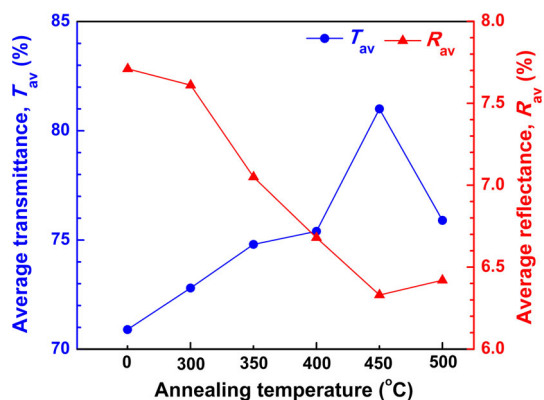

Fig. 3 A typical EDS spectrum of the AZO/Ag/FTO film annealed at 450 °C

where T_i is the transmittance value at a given wavelength, and n is the number of the transmittance values. Figure 5 displays the T_{av} values of the as-deposited and the annealed
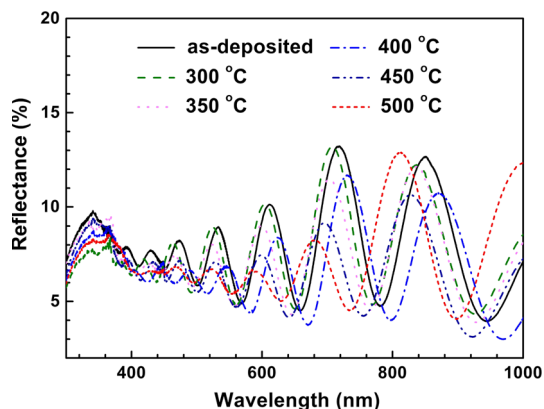

Fig. 4 Optical transmittance spectra of the as-deposited and the annealed AZO/Ag/FTO films under different temperatures

Fig. 5 Average transmittances and average reflectances (400–800 nm) of different AZO/Ag/FTO films

AZO/Ag/FTO films. The T_{av} value of the as-deposited film is 70.9%. After being annealed at 300, 350, 400, 450 and 500 °C, the films yield T_{av} values of 72.8, 74.8, 75.4, 81.0 and 75.9%, respectively. It is clearly seen that the T_{av} values of the annealed films increase at first and then decrease as the annealing temperature increases, and the maximum T_{av} value is achieved at 450 °C. This can be attributed to two aspects. On the one hand, annealing can increase the grain sizes of the films through promoting grain growth and recrystallization, which will bring about decreases in light-scattering loss at grain boundaries [31]. On the other hand, as an ideal anti-reflection coating, the AZO nanostructured layer can effectively reduce the reflected and scattered light on the film surface, which may also lead to a certain increase in transmittance of the film [10, 32]. The reflectance spectra of all the AZO/Ag/FTO films are shown in Fig. 6. In order to better describe the change tendency of the reflectance spectra, the average reflectance (R_{av}) values in the visible range (400–800 nm) for various films were obtained by applying a way similar to Eq. (2). The results are presented in Fig. 5. It is found that as compared to the as-deposited film (7.7%), the R_{av}

values of the AZO/Ag/FTO films annealed at temperatures of 300, 350, 400, 450 and 500 °C are all decreased. The change of the AZO nanostructures on the film surfaces (from needle-like whiskers to nanosheets) should be responsible for the discrepancies in R_{av} values of the films. For the AZO/Ag/FTO films annealed below 450 °C, the R_{av} values gradually decreased with increasing annealing temperature and the lowest R_{av} value (6.3%) was obtained by using an annealing temperature of 450 °C, which may be caused by the densely-distributed AZO nanosheets with larger sizes. However, the film annealed at 500 °C exhibits a slight increase in R_{av} value, which may be related to the collapsed AZO nanosheets embedded among the particles on the film surface.

3.4 Electrical property

Generally, to multilayer TCO films, a simple parallel model can be used to calculate the sheet resistance [3]. The sheet resistance (R_S) of an AZO/Ag/FTO film can be defined as the following equation:

$$\frac{1}{R_S} = \frac{1}{R_{AZO}} + \frac{1}{R_{Ag}} + \frac{1}{R_{FTO}}, \tag{3}$$

where R_{AZO}, R_{Ag} and R_{FTO} are the sheet resistances of the AZO, Ag and FTO layers, respectively. Figure 7 shows the measured sheet resistances of various AZO/Ag/FTO films. It is seen that the as-deposited film has a sheet resistance of 5.6 Ω/sq. The sheet resistances of the AZO/Ag/FTO films annealed at 300, 350, 400, 450 and 500 °C are 5.3, 5.2, 5.0, 4.7 and 4.6 Ω/sq, respectively, all lower than that of the as-deposited film. According to many reports [33, 34], the enhancement in conductivity of the annealed films is mainly attributed to the thermal annealing effect that can lead to increase in crystallite size and therefore reduce carrier scattering at grain boundaries and increase carrier mobility.

Fig. 6 Optical reflectance spectra of the as-deposited and the annealed AZO/Ag/FTO films under different temperatures
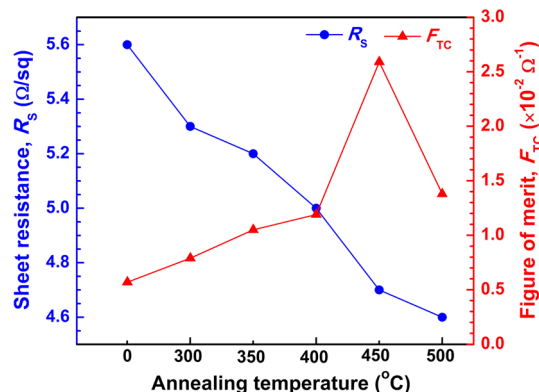
Fig. 7 Sheet resistances and figures of merit of different AZO/Ag/FTO films

In order to evaluate the AZO/Ag/FTO films and compare their overall photoelectric properties, the figure of merit (F_{TC}) is applied. F_{TC} was defined by Haacke as [35]:

$$F_{TC} = \frac{T_{av}^{10}}{R_S}, \qquad (4)$$

where T_{av} is the average transmittance and R_S is the sheet resistance. Figure 7 shows the variation of F_{TC} values for different AZO/Ag/FTO films in the wavelength range of 400–800 nm. It is well known that higher F_{TC} values represent better overall performance of the films [36]. It is found that the F_{TC} value of the as-deposited film is $0.57 \times 10^{-2} \ \Omega^{-1}$, lower than that of all the annealed AZO/Ag/FTO films. The film annealed at 450 °C has the highest figure of merit of $2.59 \times 10^{-2} \ \Omega^{-1}$, which is more than four times that of the as-deposited film, indicating that the overall photoelectric property of the as-deposited film has been greatly improved.

4 Conclusion

In summary, Ag and AZO layers were successively deposited on commercial FTO/glass substrates by DC magnetron sputtering. The as-deposited AZO/Ag/FTO film possessed an average transmittance of 70.9% (400–800 nm), a sheet resistance of 5.6 Ω/sq and a figure of merit of $0.57 \times 10^{-2} \ \Omega^{-1}$. The as-deposited film was annealed at various temperatures in a tube furnace to obtain AZO nanosheets and improve the overall photoelectric property of the film simultaneously. In the present study, the AZO/Ag/FTO film annealed at 450 °C was covered with larger and densely-distributed AZO nanosheets and exhibited the highest average transmittance of 81.0%, the lowest average reflectance of 6.3%, a sheet resistance of 4.7 Ω/sq and the highest figure of merit of $2.59 \times 10^{-2} \ \Omega^{-1}$. The results indicate that thermal annealing in the tube furnace not only can improve the overall photoelectric property of the as-deposited AZO/Ag/FTO film, but also can give rise to the formation of AZO nanosheet anti-reflection coatings so as to effectively enhance the transmittance of the film.

References

1. B.J. Li, M. Zhou, M. Ma, W. Zhang, W.Y. Tang, Effects of nanosecond laser irradiation on photoelectric properties of AZO/FTO composite films. Appl. Surf. Sci. **265**, 637–641 (2013)
2. D.G. Miao, S.X. Jiang, S.M. Shang, H.M. Zhao, Z.M. Chen, Transparent conductive and infrared reflective AZO/Cu/AZO multilayer film prepared by RF magnetron sputtering. J. Mater. Sci.: Mater. Electron. **25**, 5248–5254 (2014)
3. B.B. Straumal, A.A. Mazilkin, S.G. Protasov, A.A. Myatiev, P.B. Straumal, E. Goering, B. Baretzky, Amorphous grain boundary layers in the ferromagnetic nanograined ZnO films. Thin Solid Films **520**, 1192–1194 (2011)
4. L.J. Huang, N.F. Ren, B.J. Li, M. Zhou, A comparative study of different M (M = Al, Ag, Cu)/FTO bilayer composite films irradiated with nanosecond pulsed laser. J. Alloy. Comp. **617**, 915–920 (2014)
5. L. Dejam, S.M. Elahi, H.H. Nazari, H. Elahi, S. Solaymani, A. Ghaderi, Structural and optical characterization of ZnO and AZO thin films: the influence of post-annealing. J. Mater. Sci.: Mater. Electron. **27**, 685–696 (2016)
6. S.H. Mousavi, T.S. Müller, P.W. de Oliveira, The effects of the aluminium concentration on optical and electrical properties of AZO thin films as a transparent conductive layer. J. Mater. Sci.: Mater. Electron. **24**, 3338–3343 (2013)
7. S. Hamrit, K. Djessas, N. Brihi, B. Viallet, K. Medjnoun, S.E. Grillo, The effect of thickness on the physico-chemical properties of nanostructured ZnO: Al TCO thin films deposited on flexible PEN substrates by RF-magnetron sputtering from a nanopowder target. Ceram. Int. **42**, 16212–16219 (2016)
8. L. Gong, J. Lu, Z. Ye, Conductive Ga doped ZnO/Cu/Ga doped ZnO thin films prepared by magnetron sputtering at room temperature for flexible electronics. Thin Solid Films **519**, 3870–3874 (2011)
9. M.H. Abdullah, M. Rusop, Novel ITO/arc-TiO₂ antireflective conductive substrate for transmittance enhanced properties in dye-sensitized solar cells. Microelectron. Eng. **108**, 99–105 (2013)
10. H.W. Park, S. Ji, D.S. Herdini, H. Lim, J.S. Park, K.B. Chung, Antireflective conducting nanostructures with an atomic layer deposited an AlZnO layer on a transparent substrate. Appl. Surf. Sci. **357**, 2385–2390 (2015)
11. L. Aé, D. Kieven, J. Chen, R. Klenk, T. Rissom, Y. Tang, M.C. Lux-Steiner, ZnO nanorod arrays as an antireflective coating for Cu (In, Ga) Se₂ thin film solar cells. Prog. Photovolt: Res. Appl. **18**, 209–213 (2010)
12. D.D. Lin, H. Wu, W. Pan, Photoswitches and memories assembled by electrospinning aluminum-doped zinc oxide single nanowires. Adv. Mater. **19**, 3968–3972 (2007)
13. C.H. Hsu, D.H. Chen, Synthesis and conductivity enhancement of Al-doped ZnO nanorod array thin films. Nanotechnology **21**, 285603 (2010)
14. S. Kim, M.S. Kim, G. Nam, J.Y. Leem, Structural and blue emission properties of Al-doped ZnO nanorod array thin films grown by hydrothermal method. Electron. Mater. Lett. **8**, 445–450 (2012)
15. S. Cho, S.H. Jung, J.W. Jang, E. Oh, K.H. Lee, Simultaneous synthesis of Al-doped ZnO nanoneedles and zinc aluminum hydroxides through use of a seed layer. Cryst. Growth Des. **8**, 4553–4558 (2008)
16. B. Yuliarto, L. Nulhakim, M.F. Ramadhani, M. Iqbal, Nugraha, Suyatman, A. Nuruddin, Improved performances of ethanol sensor fabricated on Al-doped ZnO nanosheet thin films. IEEE Sens. J. **15**, 4114–4120 (2015)

17. B.B. Straumal, S.G. Protasova, A.A. Mazilkin, B. Baretzky, A.A. Myatiev, P.B. Straumal, Th Tietze, G. Schütz, E. Goering, Amorphous interlayers between crystalline grains in ferromagnetic ZnO films. Mater. Lett. **71**, 21–24 (2012)

18. F. Khan, S.H. Baek, J.H. Kim, Influence of Ag doping on structural, optical, and photoluminescence properties of nanostructured AZO films by sol–gel technique. J. Alloy. Comp. **584**, 190–194 (2014)

19. I. Volintiru, M. Creatore, B.J. Kniknie, C.I.M.A. Spee, M.C.M. van de Sanden, Evolution of the electrical and structural properties during the growth of Al doped ZnO films by remote plasma-enhanced metalorganic chemical vapor deposition. J. Appl. Phys. **102**, 043709 (2007)

20. S. Baruah, J. Dutta, Hydrothermal growth of ZnO nanostructures. Sci. Techno. Adv. Mater. **10**, 013001 (2009)

21. C. Ge, H. Li, M. Li, C. Li, X. Wu, B. Yang, Synthesis of a ZnO nanorod/CVD graphene composite for simultaneous sensing of dihydroxybenzene isomers. Carbon **95**, 1–9 (2015)

22. S. Mihaiu, I.M. Szilágyi, I. Atkinson, O.C. Mocioiu, D. Hunyadi, J. Pandele-Cusu, A. Toader, C. Munteanu, S. Boyadjiev, J. Madarász, G. Pokol, M. Zaharescu, Thermal study on the synthesis of the doped ZnO to be used in TCO films. J. Therm. Anal. Calorim. **124**, 71–80 (2016)

23. B.Y. Oh, M.C. Jeong, D.S. Kim, W. Lee, J.M. Myoung, Post-annealing of Al-doped ZnO films in hydrogen atmosphere. J. Cryst. Growth **281**, 475–480 (2005)

24. M.F. Chen, K. Lin, Y.S. Ho, Effects of laser-induced recovery process on conductive property of SnO$_2$: F thin films. Mater. Sci. Eng. B **176**, 127–131 (2011)

25. H. Klung, L. Alexander, *X-ray Diffraction Procedures* (Wiley, New York, 1962)

26. S.Y. Kuo, W.C. Chen, F.I. Lai, C.P. Cheng, H.C. Kuo, S.C. Wang, W.F. Hsieh, Effects of doping concentration and annealing temperature on properties of highly-oriented Al-doped ZnO films. J. Cryst. Growth **287**, 78–84 (2006)

27. Z.L. Wang, Zinc oxide nanostructures: growth, properties and applications. J. Phys.: Condens. Matter **16**, 829–858 (2004)

28. B.J. Li, M. Zhou, M. Ma, W. Zhang, W.Y. Tang, Effects of nanosecond laser irradiation on photoelectric properties of AZO/FTO composite films. Appl. Surf. Sci. **265**, 637–641 (2013)

29. M. Mazilu, N. Tigau, V. Musat, Optical properties of undoped and Al-doped ZnO nanostructures grown from aqueous solution on glass substrate. Opt. Mater. **34**, 1833–1838 (2012)

30. B.J. Li, L.J. Huang, N.F. Ren, X. Kong, Y.L. Cai, J.L. Zhang, Two-step preparation of laser-textured Ni/FTO bilayer composite films with high photoelectric properties. J. Alloy. Comp. **640**, 376–382 (2015)

31. R.J. Winfield, L.H.K. Koh, S. O'Brien, G.M. Crean, Excimer laser processing of ZnO thin films prepared by the sol–gel process. Appl. Surf. Sci. **254**, 855–858 (2007)

32. A. Čampa, J. Krč, J. Malmström, M. Edoff, F. Smole, M. Topič, The potential of textured front ZnO and flat TCO/metal back contact to improve optical absorption in thin Cu (In, Ga) Se$_2$ solar cells. Thin Solid Films **515**, 5968–5972 (2007)

33. M. Fallah, M.R. Zamani-Meymian, R. Rahimi, M. Rabbani, Effect of annealing treatment on electrical and optical properties of Nb doped TiO$_2$ thin films as a TCO prepared by sol–gel spin coating method. Appl. Surf. Sci. **316**, 456–462 (2014)

34. F. Wang, M.Z. Wu, Y.Y. Wang, Y.M. Yu, X.M. Wu, L.J. Zhuge, Influence of thickness and annealing temperature on the electrical, optical and structural properties of AZO thin films. Vacuum **89**, 127–131 (2013)

35. G. Haacke, New figure of merit for transparent conductors. J. Appl. Phys. **47**, 4086–4089 (1976)

36. B.J. Li, L.J. Huang, N.F. Ren, M. Zhou, Titanium dioxide-coated fluorine-doped tin oxide thin films for improving overall photoelectric property. Appl. Surf. Sci. **290**, 80–85 (2014)